Signalling centre vortices coordinate collective behaviour in social amoebae

Hugh Z Ford[1], Angelika Manhart[2] & Jonathan R Chubb[1]

[1] Laboratory for Molecular Cell Biology and Department of Cell and Developmental Biology, University College London, United Kingdom
[2] Department of Mathematics, University College London, United Kingdom

Abstract

Self-sustaining signalling waves provide a source of information in living systems. A classic example is the rotating spiral waves of cAMP (chemoattractant) release that encode *Dictyostelium* morphogenesis. These patterns remain poorly characterised due to limitations in tracking the signalling behaviour of individual cells in the context of the whole collective. Here, we have imaged *Dictyostelium* populations over millimetre length scales and track the emergence, structure, progression and biological effects of cAMP waves by monitoring the signalling states and motion of individual cells. Collective migration coincides with a decrease in the period and speed of waves that stem from an increase in the rotational speed and curvature of spiral waves. The dynamics and structure of spiral waves are generated by the vortex motion of the spiral tip. Spiral tip circulation spatially organises a small group of cells into a ring pattern, which also constrains spiral tip motion. Both the cellular ring and tip path gradually contract over time, resulting in the acceleration of spiral rotation and change in global wave dynamics. Aided by mathematical modelling, we show that this contraction is due to an instability driven by a deflection in cell chemotaxis around the spiral tip cAMP field, resulting in a deformation of the cellular ring pattern towards its centre. That is, vortex contraction modulates the source of information which, upon dissemination (excitable signal relay) and decoding (chemotaxis), triggers morphogenesis. By characterising rotating spiral waves at this level of detail, our results describe a mechanism by which information generated by a self-sustaining signal, and disseminated across the population, is modulated at the organisational source.

Introduction

Dictyostelium transition from single- to multi-cellular modes of life upon starvation [1-3]. Without a food source, cells express proteins that allow cell-cell communication via the chemoattractant cyclic adenosine monophosphate (cAMP) [4-7]. cAMP signals are relayed by excitable secretion and diffusion [8-13]. Consequently, cells secrete cAMP in spatiotemporal patterns characteristic of other excitable media [14-18]; circular wave patterns of activation first emerge and are then replaced by rotating spiral patterns [19-21]. Spiral waves are generated by the circulation of the spiral tip - a patch of cAMP secretion that periodically moves around the spiral core [22]. Rotating spiral waves produce periodic wave trains whose period and speed are set by the spiral rotation rate and curvature [22-25]. Information is carried by wave period and speed [26, 27] and decoded by cells in terms of changes in motility [28, 29] and gene expression [30-32]. Circulation of the spiral tip thus encodes the information that culminates in collective cell migration towards the spiral core and the nucleation of multicellularity [33-35].

Relative to information coding, decoding and propagation in *Dictyostelium*, the mechanism of information production and control remain poorly characterised. Chiefly, how does cell signalling, motion and spatial patterning at the spiral core modulate the period and speed of periodic cAMP wave trains that drive morphogenesis?

In this paper we use genetically-expressed reporters of cell signalling and position, time-lapse microscopy, image analysis and mathematical modelling to characterise collective cell signalling and motion during *Dictyostelium* morphogenesis with unprecedented detail. We first analyse cAMP waves patterns at the population and single cell context and relate changes in collective motion and wave dynamics generated by rotating spiral cAMP waves. By fitting spiral curves to the distribution of cell signalling states we quantify the changes in global cAMP wave dynamics due to an increase spiral wave rational speed and curvature. Finally, to determine the mechanism that controls the evolution of spiral wave structure and dynamics, we couple mathematical modelling with the simultaneous analysis of the signalling, position and motion of each cell at the spiral wave core, the organising source of global cAMP waves. Our results reveal how changes in local cell arrangement, signalling dynamics and patterns at the signalling centre can drive a sharp transition in global cell behaviour during morphogenesis.

Results and Discussion

Single-cell tracking through the transition to collective signalling

To track both the signalling and motion of individual cells during morphogenesis we imaged cells expressing a nuclear marker (H2B-mCherry) [32] together with the cAMP signalling reporter Flamindo2 [36] from endogenous genetic loci (Figure 1A and 1B). The position of each cell was measured by the central position of the nuclei and the internal [cAMP] was measured from the mean pixel intensity of the cell body (Figure 1B). This enables the cell motion and signalling of individual cells to be tracked over time (Figure 1C). Analysing all cell tracks simultaneously provides the means to study the collective motion and signalling behaviour of single cells in their population context (Figure 1D and Supplementary Movie 1).

Prior to the onset of cAMP waves (around 4 hours following starvation), cells produce cAMP pulses spontaneously at a mean rate of around 1 pulse per 12 minutes, with a minimum of 1 pulse per 3 minutes (Figure 1E). During this time, the population distribution of inter-activation intervals follows an exponential distribution offset from zero. This indicates a Poisson point process (memoryless activation events) with a fixed waiting time.

The initial cAMP waves (around 4-5 hours) are broad bands of broken waves amalgamating from numerous circular patterns that expand from spontaneously activating cells (Figure 1A). Our data show that activation events prior to synchronisation are stochastic/aperiodic, spatially variable and mostly do not initiate a cAMP wave. These observations are inconsistent with the model that individual “pacemaker” cells act as the organising source of

global cAMP waves [6]. However it may be possible that cell clusters (arising from random motion and volume exclusion [37]) may collectively act as a pacemaker if the cell cluster is sufficiently dense such that at least one cell in the cluster is likely to activate just after the refractory time [38, 39]. Nevertheless, any given cell will experience circular waves from several different sources with a variable periodicity (5-9 minutes) (Figure 1A-1D). The rate of cAMP signals produced by circular waves is inconsistent and often slower than the spontaneous firing rate. Consequently not all cells will relay a circular wave because cells that fire synchronously with one wave can potentially reactivate and so be refractory for the next wave. This is highlighted by a multi-peaked population distribution for inter-activation intervals (4-6 hours) where the peak with the smallest value is associated with spontaneous cAMP pulses while the other peaks are associated with synchronised firing during a wave (Figure 1E).

Rotating spiral cAMP waves form from broken waves around 5-6 hours following starvation (Figure 1A) [40]. Potentially the waves break as they pass a patch of cells in the refractory state. Rotating spiral patterns generate waves that are more frequent and consistent than circular patterns and hence become the dominant pattern over time, overriding the less frequent circular waves, as reported in previous studies [19-21]. The mean wave frequency steadily increases towards the maximum firing frequency of cells, around 4 minutes (Figure 1E). Consequently, the proportion of spontaneously activating cells tends to zero as there is no time to activate between waves (Figure 1D) and the population distribution of inter-pulse intervals tends to a normal distribution, with an additional peak for cells that “skip a beat” (Figure 1E). We only observed the transition to streaming in the presence of cAMP spiral waves.

Single-cell tracking though the transition to collective migration

To determine how information encoded by spiral waves coordinates collective motion, we related changes in cell chemotaxis and cAMP wave dynamics (Figure 2 and Supplementary Movie 1). A gradual change in the spatial organisation and motility of cells occurs between 6 and 8 hours following starvation, coincident with the onset of spiral waves (Figure 2A and Supplementary Figure 2). During this process, cAMP waves gradually become more frequent, slower and thinner and cells become faster, more directional and persistent in their movement (Figure 2B and 2C) [27-29]. The profile of the mean cAMP pulse is similar to previous measurements [12] and mathematical models [41, 42], and remains constant with each wave such that the wave width also decreases as the wave speed decreases [11]. Overall, the data presented in this section integrates and contextualises decades of work that focused primarily on individual components of the system in isolation.

Since cAMP is a chemoattractant, the relationship between wave dynamics and spatial order is set by cell chemotaxis [8, 9]. The following two measures are used to summarise collective cell motion: (i) the mean chemotaxis index, the proportion of cell movement in the direction of the oncoming wave (Figure 2D) [29], and (ii) the local correlation of cell velocity (Figure 2E) [43]. Cells consistently move towards the wave source at wave fronts, but remain spatially uniform prior to 6 hours due to random cell motion at the wave rear (Figure 2B). This is highlighted by a peak in the local correlation of cell motion and the mean chemotaxis index at the wave front, both of which then decay towards zero by the next wave front (indicative of random cell motion). For infrequent waves (i.e. circular patterns), these measures tend back to baseline at the following wave front, suggesting that random cell motion disrupts any order in collective cell motion gained by the front of wave. The chemotaxis index and velocity correlation strongly change as the cAMP wave frequency increases from 1 wave per 5.5 minutes to 1 wave per 3.5 minutes between 6 and 8 hours following starvation. From 6.5 hours onwards, when the wave frequency is greater than 1 per 4.5 minute, the measures of collective cell motion do not relax back to their previous values by the next wave and hence gradually increase over time to constant, elevated values across the entire wave (Figure 2D and 2E). That is, above a threshold frequency each wave causes cells to gradually exhibit more memory of their direction of motion and hence gain consistent collective motion [28, 29, 44]. In parallel, the cell speed at the front of the wave increases incrementally with each wave until it peaks at around 7μm per minute (2nd Panel Figure 2D). Cell speeds at the wave

rear only slightly increases such that the distribution of cell speed across the wave transitions from a double to single peak (at the front), associated with pulsatile collective motion in a single direction, towards the wave source (Figure 2D). Altogether, the increase in wave frequency stemming only from spiral waves periodically increases cell chemotaxis speed and memory and sufficiently accounts for the spatial order gained (streams) from 6.5 hours onwards.

Spiral wave evolution coordinates collective migration

To characterise the dynamics of the spiral waves underlying morphogenesis, we imaged and analysed the motion and signalling of individual cells around the spiral core following the onset of spiral formation (Figure 3 and Supplementary Movie 3). The spiral core is the region about which the spiral tip (the broken end of the wave) moves. The spiral tip is a patch of activation states that, by virtue of circular motion, sustains itself and the entire spiral wave (also called the spiral rotor or vortex) [22]. That is, the circulation of the spiral tip is the organising source of the spiral wave. Cells around the spiral core organise into a ring pattern that matches the path of spiral tip circulation (Figure 3A). Cells inside the spiral core do not pulse (unlike chimera spiral waves [45]) and move outwards, whereas cells outside the spiral core pulse synchronously and move inwards. The ring of cells and the circulation of the spiral tip gradually contract together, coinciding with changes in the dynamics and structure of the spiral wave. Contraction of the cellular ring results in a disk structure in which the cells rotate around the centre, a self-organised vortex state [35, 46]. These observations motivate the study of how spiral tip circulation (i) is sustained by a small group of cells (order of 100s), (ii) changes over time and (iii) encodes the information that drives morphogenesis of large number of cells (order of 100,000s).

To quantify the evolving dynamics of the spiral wave, we map the [cAMP] of individual cells to a phase variable measuring the sequence of changes in the internal [cAMP] during a pulse (which increases from π (baseline [cAMP]) to 2π, 0 (maximum [cAMP]) and then back to π) (Figure 3B). This approach reveals the spiral singularity—or topological defect [47]— which is the point in space where the full set of phase contours converge [22, 48]. To track the spiral tip, we estimate its position as the mean position of activated cells close to the phase singularity (Figure 3C). The spiral tip circulates and steadily contracts from 10-12 to 2-3 cell widths (Figure 3B, 4A and 4B), resulting in an increase in the curvature (inverse of the radius) of tip circulation. The pivotal axis meanders such that tip circulation eventually encloses adjacent to the edge of the path at the onset of spiral formation (Figure 4A). During this time, the spiral tip speed decreases from 100-120 to 40-50 μm per minute (Figure 4B). This deceleration is indicative of the dispersion relation effect where the wave speed decreases as the wave frequency increases [15, 23, 49]. That is, the wave speed decreases because cells do not fully recover during the time period taken for the signalling wave to travel once around the ring pattern of cells. The rotation rate of the spiral tip is given by the tip speed divided by the radius of circulation. The radius of circulation decreases faster than the tip speed; consequently its period of rotation (2π divided by the rotation rate) steadily decreases from around 5.5 minutes until it plateaus at 3.5 minutes (Figure 4B). Since the rotation of the spiral wave and tip are coupled [15, 33, 40], our data indicates that the reduction in the radius of spiral tip circulation drives the increase in the rotation rate of the spiral wave (Figure 4C). We also observe that spiral waves with circulating tips that are slow to contract become overridden by neighbouring spirals that generate cAMP waves at a higher frequency, much like the earlier circular waves.

To illustrate spiral tip circulation as the organising source of the spiral wave, we show how the spiral structure can be approximated by a signal that moves with speed $v_0 - \varepsilon K$ (the eikonal relation where v_0 is the base cAMP wave speed, ε is a constant and K is the curvature of spiral tip circulation) outwardly along a straight line that extends perpendicularly to the spiral tip velocity (Figure 4D) [50]. As such, tip circulation (radius and speed) modulates the spiral wave structure (curvature) and dynamics (angular velocity) and hence sets the dynamics of the train of cAMP waves that coordinate the collective motion and spatial ordering of the population (Figure 2).

To quantify the spiral structure at each point in time, we fit a simple equation for the spiral generated by continuum models of excitable media [23] to the 2π, 0 contour (maximally activated cells) of the cell phase states, starting at the spiral tip (see Figure 3C). The curvature (set by parameter k) and orientation (given by parameter θ_0) of the fitted spiral steadily changes over time (Figure 4B). Model parameter k is found to be similar to the curvature of spiral tip circulation (the inverse of its radius). Thus as the circulation of the spiral tip contracts, the spiral wave steadily becomes more curved until it plateaus around 1.5 hours after spiral formation. This observation is inconsistent with pervious observations of spiral cAMP waves [19]. For a fixed rotation rate, increasing the curvature of a rotating spiral decreases the speed and wavelength of the train of outwardly traveling cAMP waves, but not the wave period, which is modulated by the rotation rate [19, 22-25, 51]. The measured spiral curvature and rotation rate predicts a train of outwardly travelling waves whose period and speed decreases (Figure 4B) in a way that closely matches the evolving wave train dynamics measured away from the spiral core (Figure 2C). This match, together with the validated eikonal relation, consolidates spiral tip motion as the source of information disseminated across the population during morphogenesis (Figure 4C). Altogether, our results point to the contraction of spiral tip circulation as the key driver of *Dictyostelium* self-organisation.

An instability in cell chemotaxis, signalling and spatial patterning drives spiral evolution

How does the motion of the spiral tip change over time? To address this, we developed a hybrid partial differential equation (PDE) agent-based model (ABM) that encapsulates the interplay between cell motion, spiral wave dynamics and spatial patterning of cells around the spiral core (Figure 5 and Supplementary movie 4). The external [cAMP] field was modelled by a reaction-diffusion equation with constant decay rate and point source terms from the central location of each cell [15, 33]. The FitzHugh-Nagumo model was used to describe the release of cAMP from each cell [42, 52]. We tested several mathematical models of cell chemotaxis (see Supplementary Material). The model that best fit the experimental data (single cell tracks and inferred external [cAMP] field - see Supplementary Movie 3) was a simple system of linear ordinary differential equations that encapsulate chemotactic memory [28, 29]. The results presented in Figure 5 are derived from simulations of 64,000 cells randomly distributed across a 4mm x 4mm spatial domain. Refer to Supplementary Material for the full model derivation and analysis.

Without changing the previously published parameter values for cAMP release [42], we find that the hybrid model, like previous models of cAMP waves [24, 33], reproduces a rotating spiral wave and cell spatial patterning similar to experimental observations (Figure 5A and 5B). As the spiral rotates across a homogeneous spatial distribution of cells, it creates an external [cAMP] gradient inside the path of spiral tip circulation that is constantly increasing towards the spiral tip along the radial direction away from the pivot point of the spiral (Figure 5C). The converse is true for cells outside the spiral core. As such, spiral tip circulation creates a closed loop of cell motion (a limit cycle) that is similar to the path of spiral tip motion. Consequently, cells collect along the limit cycle via chemotaxis, which forms a ring pattern with radiating streams that join the ring.

Our experimental data and mathematical model both show that the cAMP wave of the spiral tip periodically travels around the ring pattern of cells in the opposite direction to cell motion (e.g. cells move clockwise and the wave moves anticlockwise). This is the active phase wave state produced by the “swarmalator” model [53]. Unlike common forms of the swarmalator model [53], previous models of cAMP waves [24, 33, 54] and continuum models of excitable media [23], the radius of spiral tip circulation and the ring pattern of cells contracts over time. It is conceivable that this contraction is driven by cellular crowding effects from cells that funnel from streams towards the spiral core. In this case, the inward collective motion of cells would provide a force that drives a contraction of the ring pattern of cells and hence also the radius of spiral trip circulation. However a similar contraction rate of spiral tip circulation can be observed in simulations without a repulsive force between cells, showing that this hypothesis is not sufficient to explain the data (third panel of Figure 5E and 5F). It is also conceivable that spiral tip circulation might naturally contract independently of the distribution of cells. In this case, the distribution of cells would simply mirror the spiral trip path without influencing it. However spiral tip circulation

holds a fixed radius (like in continuum models of spiral waves [23]) in simulations without cell motion, showing that this hypothesis is also not sufficient to explain the data (second panel of Figure 5E and 5F). Rather, the simulations strongly suggest that the contraction of spiral tip circulation arises from an instability where (i) the ring pattern of cells constrains spiral tip motion and (ii) the external [cAMP] field around the spiral tip "pulls" cells inwards from the ring edge (Figure 5D). In this mechanism, the spiral tip deflects the circular path of cell motion inwards, resulting in a ring that appears blunted around the inner leaflet of the spiral tip (fourth panel of Figure 3A and second panel of Figure 5B and 5C). If the blunted region of the ring pattern of cells at the wave rear does not relax back to its previous state at the wave front during each period of rotation, then the ring pattern of cells and spiral tip circulation will steadily contract together.

To observe the instability in cell chemotaxis, signalling and spatial patterning in the experimental data, we consider the mean spatial distribution of cell activity (Figure 6A), velocity (Figure 6B) and density (Figure 6C) about the spiral wave. We use a rotating reference frame that is centred at the spiral pivotal axis and rotating with the spiral tip such that the spiral appears motionless (bar curvature evolution). This reference frame reveals the heterogeneity in cell spatial patterning and chemotaxis around the spiral core. Analysis of streamlines across the mean cell velocity field outlines the emergence of the limit cycle in cell motion (Figure 6B). The limit cycle appears around 30 minutes after spiral wave formation, and its minimum and mean distance from the spiral pivotal axis consistently lie on either side of the radius of spiral tip circulation. The limit cycle increases the cell density around the path of tip circulation, which is shifted slightly (1-3 cell widths) inwards from the crest (Figure 6C). Consistent with the simulations (Figure 5), the minimum distance between the limit cycle and pivotal axis is constantly orientated towards the spiral tip, which highlights how cell chemotaxis is deflected around the external [cAMP] field of the spiral tip, inwards from the edge of the cell ring (Figure 6B and 6C). This match between the simulations and experimental data strongly suggests that the instability in cell chemotaxis, signalling and spatial patterning around the spiral core (Figure 5D) is the mechanism driving the contraction of spiral tip circulation, and hence also the increase in spiral rotation rate and curvature (Figure 4C).

Conclusion

We have carried out an in-depth characterisation of collective signalling and motion during *Dictyostelium* morphogenesis. Our analysis shows how information disseminated as a rotating spiral wave is generated, encoded and modulated by the circulation of the spiral tip - the signal vortex. The speed and period of the global periodic wave trains are set by spiral wave curvature and rotation rate, which are inversely proportional to the vortex radius. The vortex contracts due to an instability in the patterning of cell arrangement and signalling. Cells form a ring pattern by chemotaxis towards the circulating external [cAMP] field, which becomes fastened to the ring of cells. In this state, the external [cAMP] field deflects cell chemotaxis towards the axis of circulation, resulting in the steady contraction of the cellular ring and signal vortex. Cells decode information in terms of chemotaxis; a change in information encoded locally at the signalling centre results in a sudden gain of global collective cell migration towards the spiral core, the key event of the morphogenesis programme. Our study suggests a new mechanism by which global self-sustaining signals can be controlled locally by a small subset of the cell population.

Methods

Generation of cell line

AX3 *Dictyostelium* were engineered to express Flamindo2 and H2B-mCherry from safe haven genomic locations. Flamindo2 is a cAMP biosensor [36] with a fluorescence intensity that is inversely proportional to internal cAMP levels. The Flamindo2 reporter is knocked-in to the a*ct5* locus for stable and uniform expression [55, 56]. H2B-mCherry, knocked into the *rps30* locus, labels the nucleus for cell tracking at high cell densities [32].

Cell culturing

Cells (AX3) were grown at 22ºC in the Formedium HL5 medium supplemented with penicillin and streptomycin. Cultures were diluted to 1/4 per day to negate cell entry to stationary phase. Cells were not used beyond 10 days of culture. For development, log-phase cells at 80% confluency were washed and resuspended in KK2 (20 mM KPO4 pH 6.0), and then plated on 1.5% agar between 4x10^3 and 5x10^3 cells per mm^2. After 1 hour in a humidified chamber, a 1cm^2 slab of agar was cut and gently place cell-face-down onto a glass imaging dish, and then submerged in silicon oil to prevent desiccation.

Cell imaging

Cells were imaged at 22ºC on a custom built inverted wide field microscope, equipped with Prime 95B CMOS camera (Photometrics), 10x UplanFL N objective (Olympus) and 470 nm and 572 nm LED light sources (Cairn Research) [57]. A 1.2mm x 1.2mm area was imaged at resolution 1μm^2 per pixel every 4 seconds for 8 hours from 2 hours after starvation. To image cell motion and signalling about the spiral core, we begin imaging at the formation of the spiral wave, between 5 and 6 hours after starvation.

Cell tracking

The following image analysis pipeline was implemented in Matlab 2020b. To track individual cells, the IDL particle tracking algorithm [58] was applied to the cell nuclei channel (H2B-mCherry) of the image stack. The velocity of each cell at each time point was estimated by the first derivative, second order, central finite difference of cell position. To measure the mean fluorescence intensity of each tracked cell, watershed segmentation (the Fernand Meyer algorithm [59]), seeded from the tracked cell positions, was applied to the cell body channel (Flamindo2). To infer internal cAMP levels (nondimensional), the tracked mean fluorescent intensity of each cell was normalised and smoothed using Matlab's Savitzky-Golay finite impulse response smoothing filter. Two measures were used to identify cAMP pulses: (i) the similarity between the normalised intensity and a square pulse of length 2 minutes and (ii) the signalling phase φ. Variable φ was estimated by stratifying the time series of the internal cAMP level c by its time derivate $\dot{c}$ (estimated by the first derivative, second order, central finite difference). The value of φ is set as the angle around the point $c = c^*$ ($\min c < c^* < \max c$) and $\dot{c} = 0$:

$$\varphi = 2 \arctan \frac{c - c^*}{\dot{c} + \sqrt{(c - c^*)^2 + \dot{c}^2}} .$$

As such, the phase variable increases from $\varphi = \pi$ (baseline cAMP) to $\varphi = 2\pi,0$ (maximum cAMP) and then back to $\varphi = \pi$ during each pulse. The half-maximal cAMP levels were used to define the time points of cell activation ($\dot{c} > 0$) and deactivation ($\dot{c} < 0$).

Measuring collective behaviours

The time and place of activation for each cell was clustered in three dimensions (two spatial, one temporal) using the DBSCAN (density-based clustering of applications with noise) algorithm [60] as a means to identify subsets of cells with correlated signalling states (e.g. during the propagation of cAMP waves) and also, by exclusion, the cells that activate independently. To analyse the behaviour of single cells during stable periodic waves, we estimate the front, peak and back of the cAMP waves by fitting the equation for a cone to activation and deactivation times in three dimensions. The slope of the fitted cone we deduce the mean speed of each wave. The distribution of the internal [cAMP] and velocity of each cell was estimated using the fitted cone equation. The following two formulae were used to measure collective cell motion: (i) the mean chemotaxis index (the proportion of cell movement in the direction of the oncoming wave):

$$\frac{1}{N} \sum_i \hat{\mathbf{v}}_i \cdot \hat{\mathbf{w}}(\mathbf{x}_i)$$

where $\hat{\mathbf{v}}_i$ is the normal velocity of cell $i = 1,\ldots,N$ and $\hat{\mathbf{w}}(\mathbf{x}_i)$ is the normal velocity of the cAMP wave at the location of cell i, $\mathbf{x}_i$ [29], and (ii) the local correlation of cell velocity:

$$\frac{1}{N}\sum_i \sum_{j\neq i} \hat{\mathbf{v}}_i \cdot \hat{\mathbf{v}}_j$$

where the index j denotes cells within the neighbourhood of cell i [43].

Spiral wave analysis

To quantify the evolving dynamics of the spiral wave, we first estimated the location of the spiral phase singularity at each time point as the central point of a circular region with the largest variance in internal [cAMP] across each cell. The location of the spiral tip was estimated by the mean position of maximally activated cells ($\varphi \approx 2\pi$,0) closest to the location of the phase singularity. We fit the following spiral equation to the spatial distribution of maximally activated cells to the spatial position of cells close to the signalling phase of maximally activated cells ($\varphi \approx 2\pi$,0) [23]:

$$x = x_i + r\cos(\theta)\ ,\ \ y = y_i + r\sin(\theta)\ ,\ \ \theta = m\Big(kr + \log\big(\sqrt{3}+kr\big)\Big) + \theta_0\ ,$$

which is derived from the structure of rotating spiral activation waves across continuous excitable media. Here, variables x and y denote the Cartesian coordinates and variables r and θ represent the polar coordinates of the spiral. The rotation rate was determined by the time derivative (second order finite difference) of parameter θ_0 and the curvature was inferred from parameter k. As in Ref [23], constant $m = (3-\sqrt{3})/4$. To estimate the mean cell velocity field and density around the spiral wave, we measured the mean velocity and total number of cells at regular lattice areas in the reference frame that rotates with the fitted spiral parameter θ_0. The streamlines across this field were analysed using the Matlab function streamlines.

Mathematical model

A hybrid partial differential equation (PDE) agent-based model (ABM) was developed to study the interplay between cell motion, spiral wave dynamics and spatial patterning of cells around the spiral core. The 2D external [cAMP] field c was modelled by the following reaction-diffusion equation [15, 33]:

$$\partial_t c = D\,\nabla^2 c - \beta\, c + \sigma \sum_{i=1}^{N} H(A_i)\,\delta(\mathbf{x}-\mathbf{X}_i)\ \ ,$$

where β and σ are the rates of external cAMP decay and release from individual cells, D is the external cAMP diffusion coefficient, N is the number of cells, H is the Heaviside function, δ is the Dirac delta function, modelling the point source release of cAMP from cell i $(1 \leq i \leq N)$, with position $\mathbf{X}_i$ and activation state A_i. We used the same parameter values as in Ref. [39]. The following modified FitzHugh-Nagumo model was used to describe the excitable release of cAMP from each cell:

$$\tau \dot{A}_i = A_i - \frac{1}{3}A_i^3 - I_i + \alpha\log\Big(1+\frac{c_i}{\kappa}\Big)\ ,\ \ \tau\dot{I}_i = \epsilon\big(A_i - \gamma I_i + \mu\big)\ ,$$

where I_i is the inhibitor level of cell i, and the value of each parameter was the same as Ref. [42, 52], with exception of the time scale τ which was adjusted to match experimental data. We tested several mathematical models of cell chemotaxis against the data for the velocity of individual cells as a function of the external cAMP field. The external cAMP field was inferred in our experimental data by substituting the measured position and discretised activation state of each cell in the reaction-diffusion equation above, which provides a prediction for the external [cAMP] at the location of each cell $c_i = c_i(\mathbf{X}_i(t), t)$ and the spatial gradient $|c_i|$ (Supplementary Movie 3). The model that best fit the experimental data was a simple system of linear ordinary differential equations that encapsulate chemotactic memory [29]:

$$\dot{\theta}_i = \alpha_m s_i |\nabla c_i| \sin(\theta_i^c - \theta_i)\ ,\ \ \dot{v}_i = \beta_m s_i |\nabla c_i| - \gamma_m v_i\ ,\ \ \dot{s}_i = \sigma_m(1-s_i) - \lambda_m c_i s_i,$$

where θ_i and v_i are the direction and speed of cell movement and and s_i is the sensation variable to external cAMP as used in Ref. [33]. Variable and θ_i^c is the direction of the external [cAMP] spatial gradient and model parameters α_m, β_m, γ_m, σ_m and λ_m were optimised using the Matlab function fminsearch to obtained the best fit experimental data. For the final cell movement model

we also model size exclusion effects between cells, by including a cell-cell repulsion term. Model equations were solved numerically using Matlab. The external [cAMP] field was solved across a 50 grid points per mm length with the finite difference, impact Euler method in time and central difference in space. Cell velocities and activation states were solved using the Matlab function ode45. Refer to Supplementary Material for the full model derivation and analysis.

Figures

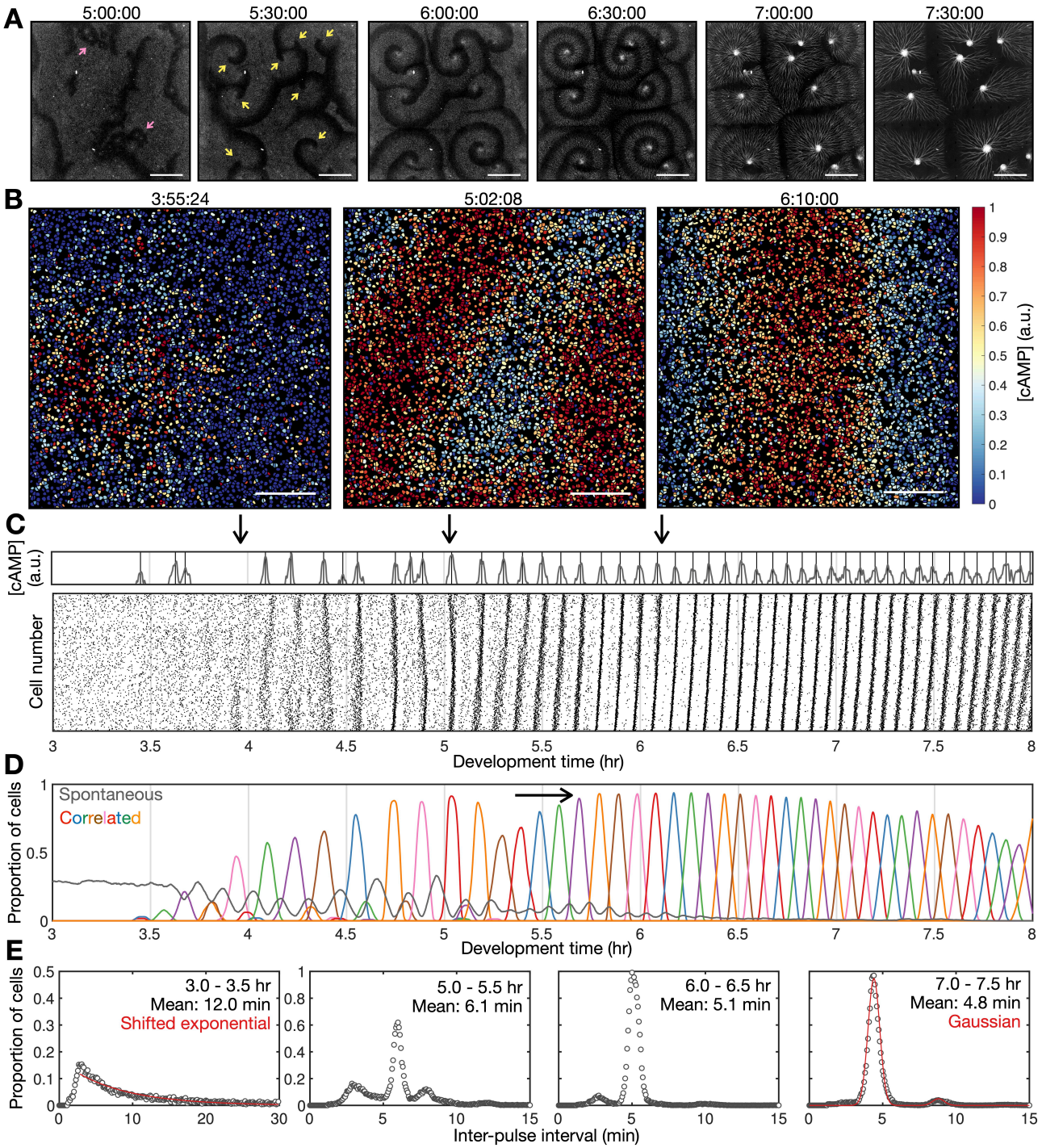

Figure 1 Signal synchronisation. A cAMP waves (dark bands) shown at 30 min intervals following 5 hours from starvation. Arrows indicate circular waves (pink) and spiral waves (yellow). Scale bar: 2mm. **B** The distribution of cells and internal [cAMP] (colour) shown at 1 hour intervals following 4 hours from starvation. Scale bar: 200 μm. **C** Representative time series of the internal [cAMP] within an individual cell (grey) with signal peaks highlighted (black) (top) and a plot of signal peaks for 1000 cells (bottom). **D** Proportion of correlated (coloured) and spontaneous (grey) activation events; each colour represents a single cAMP wave. Arrow: onset of spiral formation. **E** The distribution of inter-pulse intervals over different 30 minute time intervals (grey) with fitted shifted exponential and gaussian functions (red).

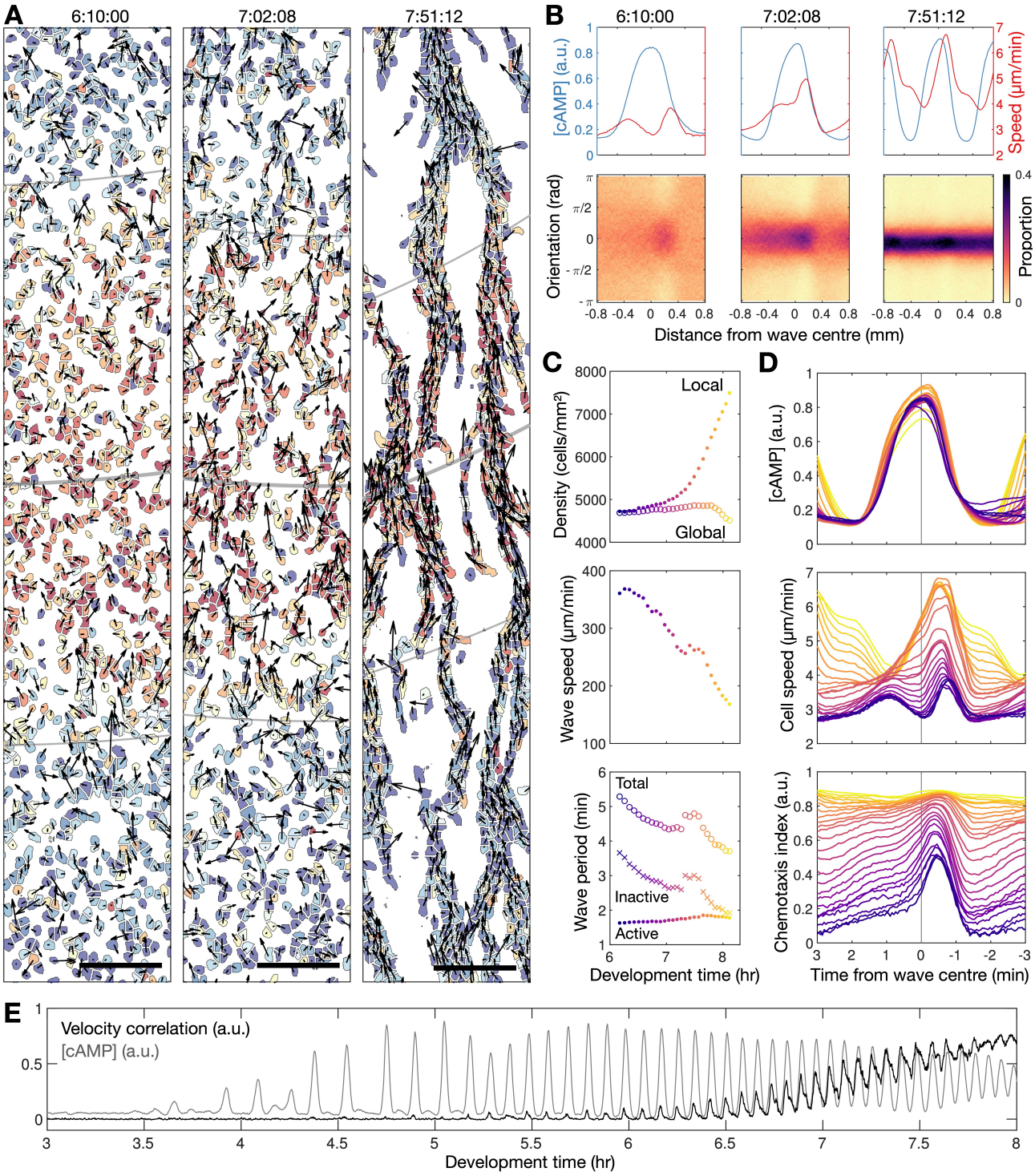

Figure 2 Collective cell motion. **A** Snapshots of cell velocities and signal states (coloured by [cAMP], see Fig 1B) surrounding a cAMP wave (travelling from top to bottom) at 3 different time points following spiral wave formation. The inferred wave boundaries and peak are highlighted as grey lines. Scale bar: 100μm. **B** The mean cell [cAMP] (blue) and speed (red) (top), and the population density distribution across the difference between the direction of cell and wave motion (0 - facing the wave), all as a function of distance from the wave centre for the three cAMP waves shown in A. **C** The local (mean) and global population density (top), wave speed (middle) and wave period (bottom) for each wave during 6 to 8 hours following starvation. Each data point is coloured by wave number. **D** The mean cell [cAMP] (top), speed (middle) and chemotaxis index (bottom) across each wave, represented as the time to the wave centre (positive - behind the wave). Each line is coloured by wave number as in C. **E** The mean cell [cAMP] (grey) and local velocity correlation (black) for cells within a 400μm² area.

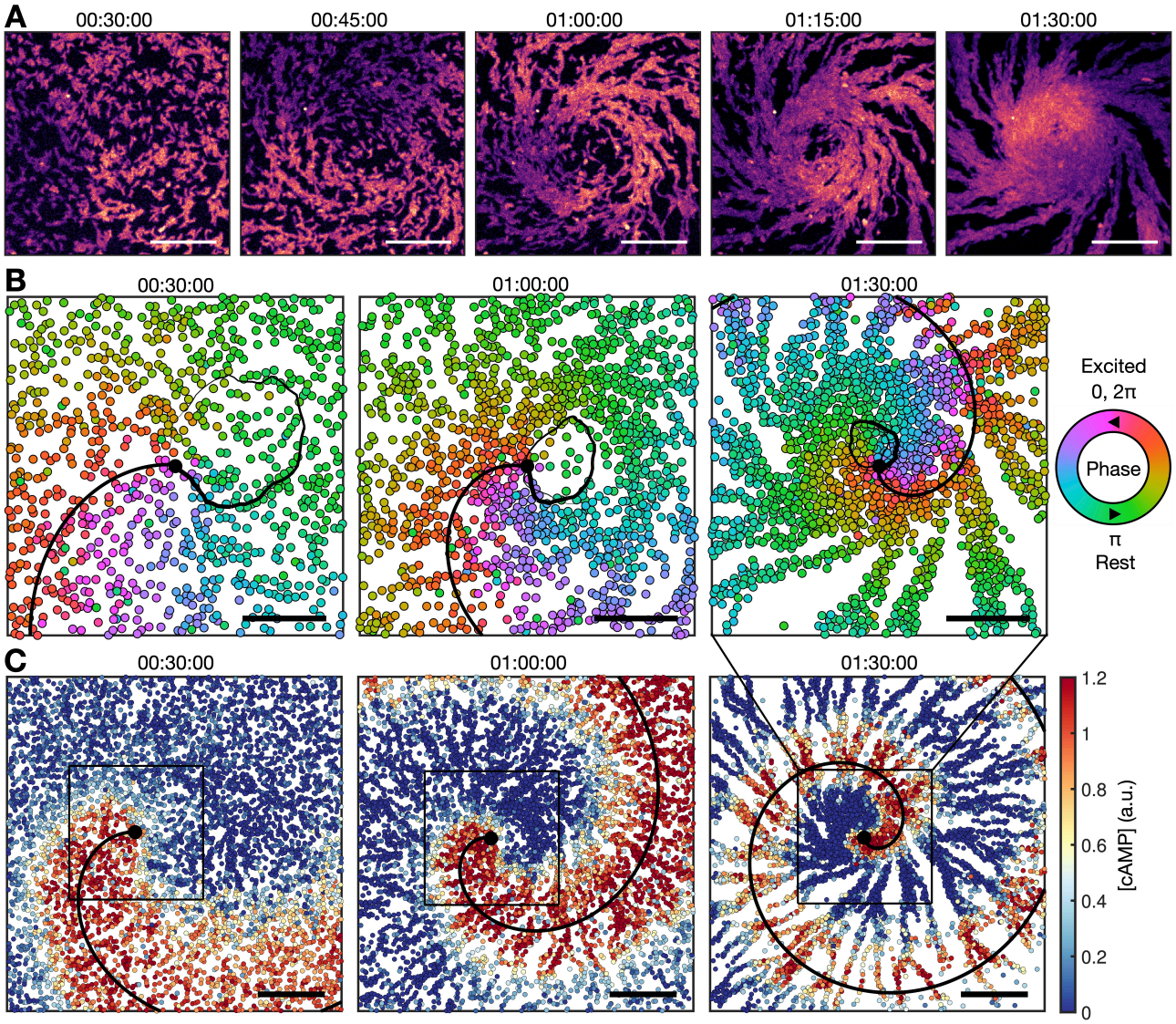

Figure 3 Spiral wave dynamics. **A** Representative images of the internal [cAMP] (yellow - low, purple - high) distributed across cells around the spiral core at 15 minute time intervals, 30 minutes from the onset of spiral formation. Scale bar: 100μm. **B** The central positions of cells (circles) coloured by their signalling phase state (red - 0,2π (maximally active) and green - π (rest)) at 3 of the same time points shown in A. Also shown is a track of the predicted spiral tip position (fading black line) and the fitted spiral shown is shown as a thick black line. Scale bar: 100μm. **C** The same as B except the cells are coloured by their [cAMP]. Scale bar: 200μm.

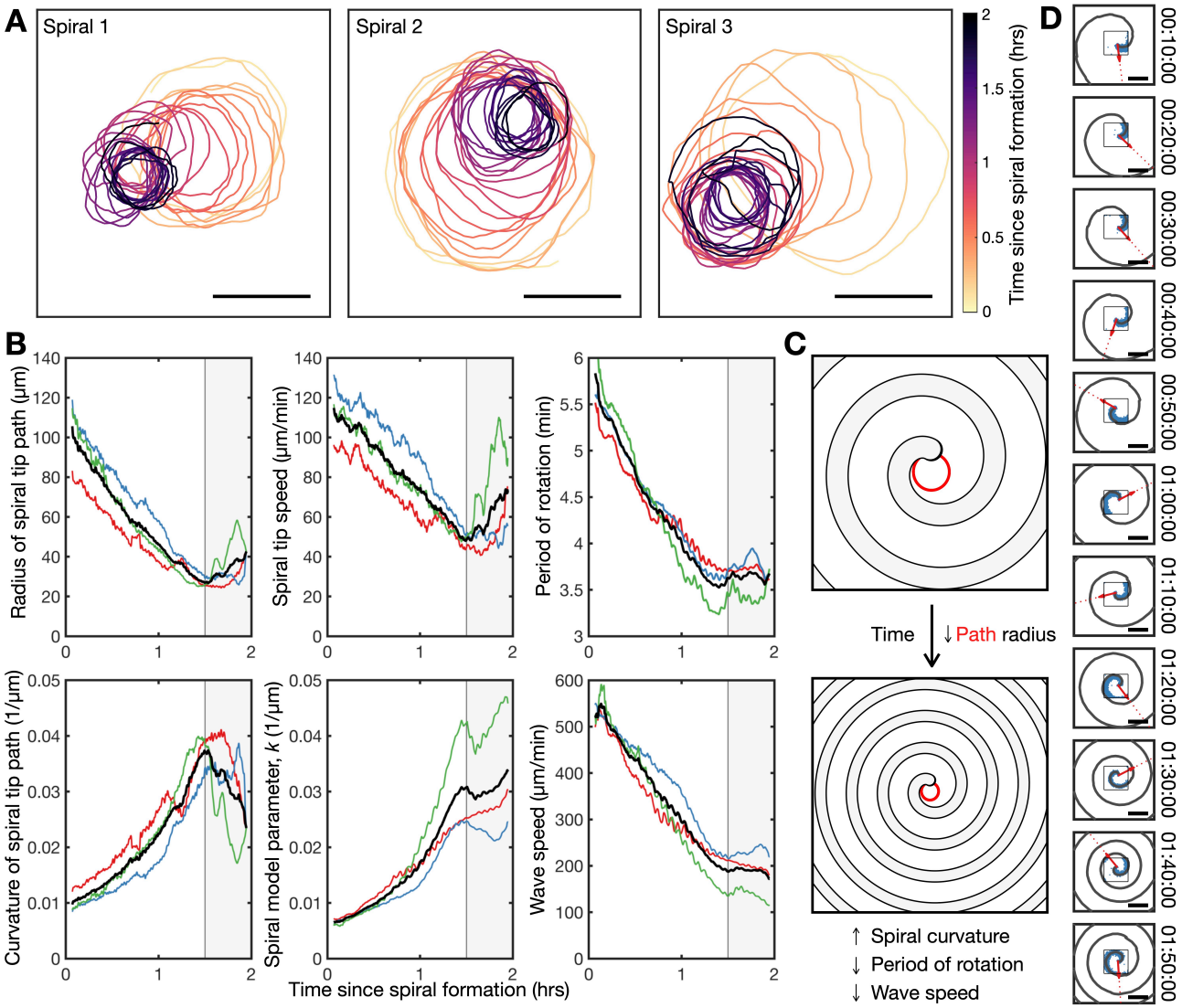

Figure 4 Spiral wave dynamics. **A** The path of spiral tip circulation for 3 spirals, coloured by the time since spiral formation. Scale bar: 100μm. **B** The radius and curvature of the path of spiral tip circulation together with its speed and period of rotation for the three spiral shown in A (red, green and blue) together with the mean (black). Also shown are the results of the spiral fit (equation (x)); model parameter k, which determined spiral curvature, and the wave speed (10^6 μm away from spiral core). **C** Cartoon schematic of the increased spiral curvature (and hence decreased wave speed) as a consequence of the decrease in path radius decreases. **D** The spiral (black line) produced by a signal moving in the normal direction (red arrow) of spiral tip motion. Also shown are the subset of active cells (blue). Scale bar: 1mm.

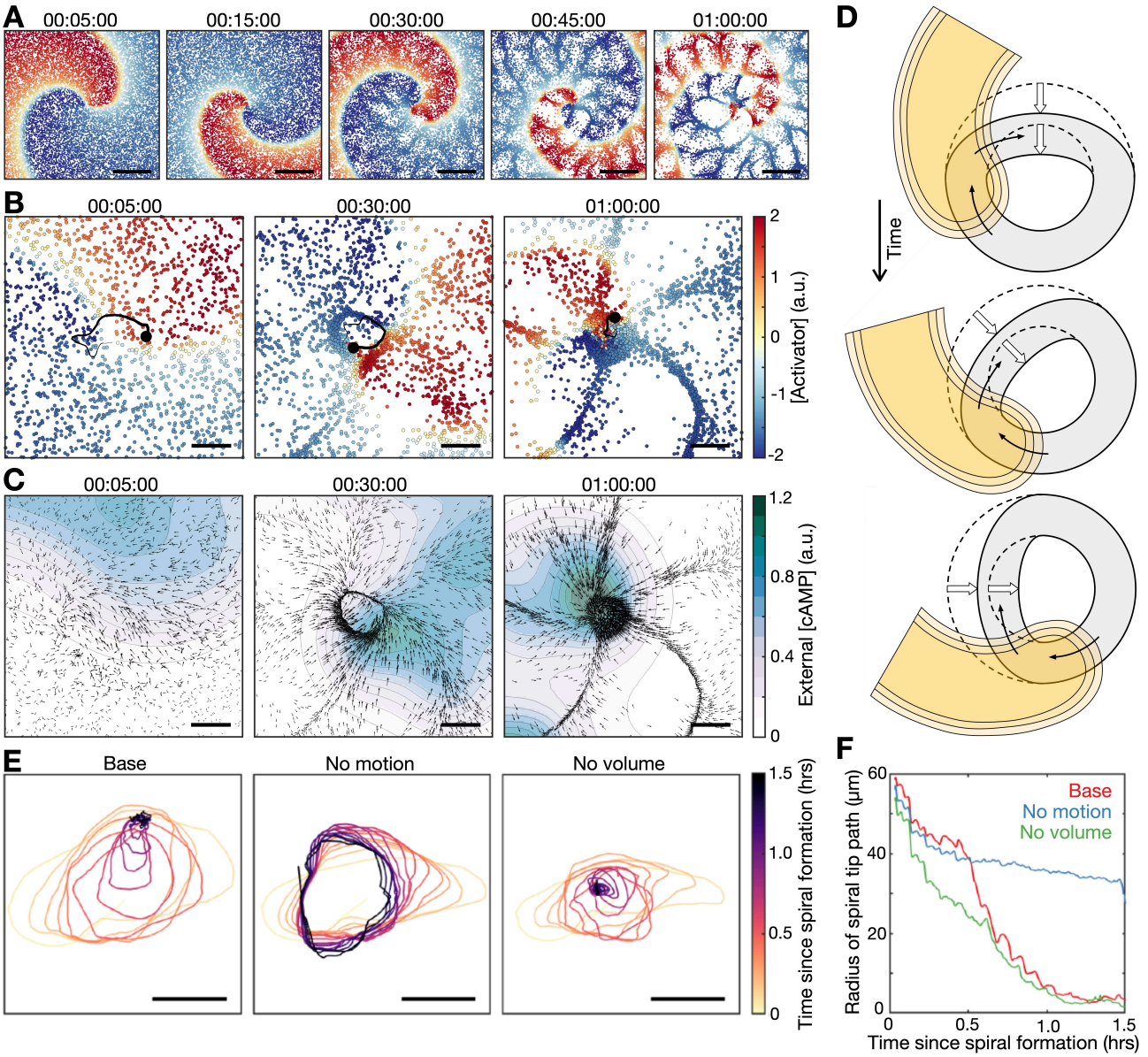

Figure 5 Mathematical model of spiral wave evolution. **A** Simulation of the cell population distribution across space and [activator] (colour). Scale bar: 500 μm. **B** Same as A together with the track (black line) of the spiral tip (black circle). Scale bar: 100 μm. **C** Evolution of the external [cAMP] field (colour) with cell velocities (black arrows) Scale bar: 100 μm. **D** Schematic of the mechanism of spiral tip contraction; as the spiral tip travels around the ring pattern of cells (grey), its external [cAMP] field (yellow) deflect cell motion (black arrow) inwards from the ring, resulting in the deformation (white arrow) of the ring behind the spiral tip. **E** Tracks of the spiral tip (coloured by time) for the base simulation (shown in A-C), a simulation without cell motion (second panel) and cell-cell volume exclusion (third panel). Scale bar: 50 μm. **F** Time series of the radius of spiral tip circulation for the tracks presented in E.

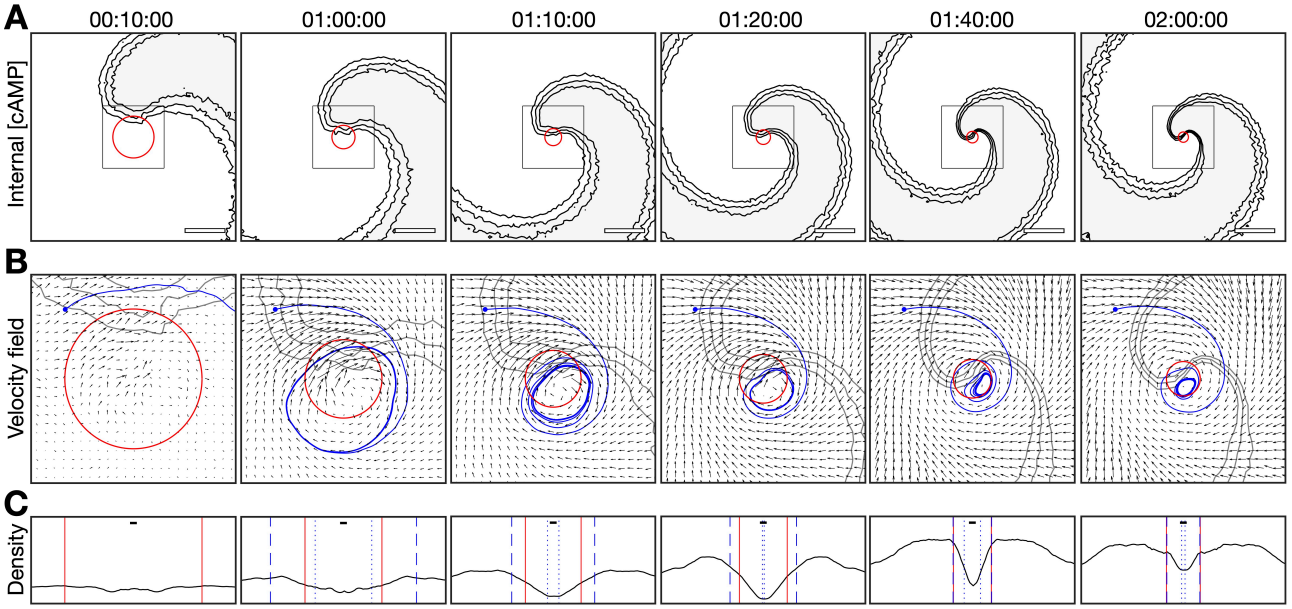

Figure 6 Contraction of spiral tip circulation. **A** The mean internal [cAMP] (a.u.) obtained in the rotating reference frame of the spiral with the mean radius of the path of phase singularity motion (red). Each plot represents a 7.5min average up to the indicated time point from spiral formation. The spiral axis of rotation is the centre of the frame. Scale bar 200μm. **B** Mean cell velocity field (arrows, 300μm x 300μm) associated with the data presented in A (highlighted by the box in A), together with a representative stream line (blue), the mean radius of the path of phase singularity motion (red) and outline of the spiral (grey). **C** The mean spatial distribution (300μm) of cell density (a.u.) across the spiral axis of rotation (black) together with the mean radius of the path phase singularity motion (red) and the minimum (dotted) and maximum (dashed) distance of the representative streamline (shown in B) from the axis of spiral rotation (blue). Scale bar: 10μm (typical cell diameter).

Bibliography

1. Bonner, J.T., A descriptive study of the development of the slime mold Dictyostelium discoideum. American Journal of Botany, 1944: p. 175-182.
2. Gerisch, G., Cell aggregation and differentiation in Dictyostelium, in Current topics in developmental biology. 1968, Elsevier. p. 157-197.
3. Weijer, C.J., *Dictyostelium morphogenesis.* Current opinion in genetics & development, 2004. **14**(4): p. 392-398.
4. Bonner, J., et al., Acrasin, Acrasinase, and the sensitivity to acrasin in Dictyostelium discoideum. Developmental biology, 1969. **20**(1): p. 72-87.
5. Tomchik, K. and P. Devreotes, Adenosine 3', 5'-monophosphate waves in Dictyostelium discoideum: a demonstration by isotope dilution--fluorography. Science, 1981. **212**(4493): p. 443-446.
6. Gregor, T., et al., The onset of collective behavior in social amoebae. Science, 2010. **328**(5981): p. 1021-1025.
7. Loomis, W.F., Cell signaling during development of Dictyostelium. Developmental biology, 2014. **391**(1): p. 1-16.
8. Nanjundiah, V., Chemotaxis, signal relaying and aggregation morphology. Journal of Theoretical Biology, 1973. **42**(1): p. 63-105.
9. Alcantara, F. and M. Monk, Signal propagation during aggregation in the slime mould Dictyostelium discoideum. Microbiology, 1974. **85**(2): p. 321-334.
10. Shaffer, B., Secretion of cyclic AMP induced by cyclic AMP in the cellular slime mould Dictyostelium discoideum. Nature, 1975. **255**(5509): p. 549-552.
11. Gross, J., M. Peacey, and D. Trevan, Signal emission and signal propagation during early aggregation in Dictyostelium discoideum. Journal of cell science, 1976. **22**(3): p. 645-656.
12. Roos, W., C. Scheidegger, and G. Gerisch, Adenylate cyclase activity oscillations as signals for cell aggregation in Dictyostelium discoideum. Nature, 1977. **266**(5599): p. 259-261.
13. Dinauer, M.C., S.A. MacKay, and P.N. Devreotes, Cyclic 3', 5'-AMP relay in Dictyostelium discoideum III. The relationship of cAMP synthesis and secretion during the cAMP signaling response. The Journal of Cell Biology, 1980. **86**(2): p. 537-544.
14. Durston, A., Dictyostelium discoideum aggregation fields as excitable media. Journal of theoretical biology, 1973. **42**(3): p. 483-504.
15. Tyson, J.J., et al., Spiral waves of cyclic AMP in a model of slime mold aggregation. Physica D: Nonlinear Phenomena, 1989. **34**(1-2): p. 193-207.
16. Meron, E., Pattern formation in excitable media. Physics reports, 1992. **218**(1): p. 1-66.
17. Höfer, T., J.A. Sherratt, and P.K. Maini, Dictyostelium discoideum: cellular self-organization in an excitable biological medium. Proceedings of the Royal Society of London. Series B: Biological Sciences, 1995. **259**(1356): p. 249-257.
18. Van Oss, C., et al., Spatial pattern formation during aggregation of the slime moulddictyostelium discoideum. Journal of theoretical biology, 1996. **181**(3): p. 203-213.
19. Foerster, P., S. Muller, and B. Hess, Curvature and spiral geometry in aggregation patterns of Dictyostelium discoideum. Development, 1990. **109**(1): p. 11-16.
20. Lee, K.J., E.C. Cox, and R.E. Goldstein, Competing patterns of signaling activity in Dictyostelium discoideum. Physical review letters, 1996. **76**(7): p. 1174.
21. Lauzeral, J., J. Halloy, and A. Goldbeter, Desynchronization of cells on the developmental path triggers the formation of spiral waves of cAMP during Dictyostelium aggregation. Proceedings of the National Academy of Sciences, 1997. **94**(17): p. 9153-9158.
22. Winfree, A.T., *The geometry of biological time*. Vol. 12. 2001: Springer Science & Business Media.
23. Tyson, J.J. and J.P. Keener, Singular perturbation theory of traveling waves in excitable media (a review). Physica D: Nonlinear Phenomena, 1988. **32**(3): p. 327-361.
24. Gerhardt, M., H. Schuster, and J.J. Tyson, A cellular automation model of excitable media including curvature and dispersion. Science, 1990. **247**(4950): p. 1563-1566.
25. Fast, V.G. and A.G. Kleber, Role of wavefront curvature in propagation of cardiac impulse. Cardiovascular research, 1997. **33**(2): p. 258-271.

26. Siegert, F. and C. Weijer, Digital image processing of optical density wave propagation in Dictyostelium discoideum and analysis of the effects of caffeine and ammonia. Journal of Cell Science, 1989. **93**(2): p. 325-335.
27. Siegert, F. and C.J. Weijer, Analysis of optical density wave propagation and cell movement in the cellular slime mould Dictyostelium discoideum. Physica D: Nonlinear Phenomena, 1991. **49**(1-2): p. 224-232.
28. Fisher, P., R. Merkl, and G. Gerisch, Quantitative analysis of cell motility and chemotaxis in Dictyostelium discoideum by using an image processing system and a novel chemotaxis chamber providing stationary chemical gradients. Journal of Cell Biology, 1989. **108**(3): p. 973-984.
29. Skoge, M., et al., *Cellular memory in eukaryotic chemotaxis.* Proceedings of the National Academy of Sciences, 2014. **111**(40): p. 14448-14453.
30. Mehdy, M.C., D. Ratner, and R.A. Firtel, Induction and modulation of cell-type-specific gene expression in Dictyostelium. Cell, 1983. **32**(3): p. 763-771.
31. Gomer, R.H., et al., cAMP induction of prespore and prestalk gene expression in Dictyostelium is mediated by the cell-surface cAMP receptor. Proceedings of the National Academy of Sciences, 1986. **83**(22): p. 8624-8628.
32. Corrigan, A.M. and J.R. Chubb, Regulation of transcriptional bursting by a naturally oscillating signal. Current Biology, 2014. **24**(2): p. 205-211.
33. Höfer, T., J.A. Sherratt, and P.K. Maini, Cellular pattern formation during Dictyostelium aggregation. Physica D: Nonlinear Phenomena, 1995. **85**(3): p. 425-444.
34. Dormann, D., B. Vasiev, and C.J. Weijer, Propagating waves control Dictyostelium discoideum morphogenesis. Biophysical chemistry, 1998. **72**(1-2): p. 21-35.
35. Rappel, W.-J., et al., Self-organized vortex state in two-dimensional Dictyostelium dynamics. Physical review letters, 1999. **83**(6): p. 1247.
36. Odaka, H., et al., Genetically-encoded yellow fluorescent cAMP indicator with an expanded dynamic range for dual-color imaging. PloS one, 2014. **9**(6): p. e100252.
37. Liu, G., et al., Self-driven phase transitions drive Myxococcus xanthus fruiting body formation. Physical review letters, 2019. **122**(24): p. 248102.
38. Mirollo, R.E. and S.H. Strogatz, Synchronization of pulse-coupled biological oscillators. SIAM Journal on Applied Mathematics, 1990. **50**(6): p. 1645-1662.
39. Vidal-Henriquez, E. and A. Gholami, Spontaneous center formation in Dictyostelium discoideum. Scientific reports, 2019. **9**(1): p. 1-11.
40. Mikhailov, A., V. Davydov, and V. Zykov, Complex dynamics of spiral waves and motion of curves. Physica D: Nonlinear Phenomena, 1994. **70**(1-2): p. 1-39.
41. Martiel, J.-L. and A. Goldbeter, A model based on receptor desensitization for cyclic AMP signaling in Dictyostelium cells. Biophysical journal, 1987. **52**(5): p. 807-828.
42. Sgro, A.E., et al., From intracellular signaling to population oscillations: bridging size-and time-scales in collective behavior. Molecular systems biology, 2015. **11**(1): p. 779.
43. De Palo, G., D. Yi, and R.G. Endres, A critical-like collective state leads to long-range cell communication in Dictyostelium discoideum aggregation. PLoS biology, 2017. **15**(4): p. e1002602.
44. Bretschneider, T., H.G. Othmer, and C.J. Weijer, Progress and perspectives in signal transduction, actin dynamics, and movement at the cell and tissue level: lessons from Dictyostelium. Interface Focus, 2016. **6**(5): p. 20160047.
45. Totz, J.F., et al., Spiral wave chimera states in large populations of coupled chemical oscillators. Nature Physics, 2018. **14**(3): p. 282-285.
46. Nicol, A., et al., Cell-sorting in aggregates of Dictyostelium discoideum. Journal of cell science, 1999. **112**(22): p. 3923-3929.
47. Shankar, S., et al., *Topological active matter.* arXiv preprint arXiv:2010.00364, 2020.
48. Allessie, M.A., F.I. Bonke, and F.J. Schopman, Circus movement in rabbit atrial muscle as a mechanism of tachycardia. Circulation research, 1973. **33**(1): p. 54-62.
49. Dockery, J. and J. Keener, Diffusive effects on dispersion in excitable media. SIAM Journal on Applied Mathematics, 1989. **49**(2): p. 539-566.
50. Keller, J.B., Geometrical theory of diffraction. Josa, 1962. **52**(2): p. 116-130.
51. Foerster, P., S.C. Müller, and B. Hess, Curvature and propagation velocity of chemical waves. Science, 1988. **241**(4866): p. 685-687.
52. Huyan, C., et al., Robust coordination of collective oscillatory signaling requires single-cell excitability and fold-change detection. bioRxiv, 2021.

53. O'Keeffe, K.P., H. Hong, and S.H. Strogatz, *Oscillators that sync and swarm.* Nature communications, 2017. **8**(1): p. 1-13.
54. Noorbakhsh, J., et al., Modeling oscillations and spiral waves in Dictyostelium populations. Physical Review E, 2015. **91**(6): p. 062711.
55. Paschke, P., et al., Rapid and efficient genetic engineering of both wild type and axenic strains of Dictyostelium discoideum. Plos one, 2018. **13**(5): p. e0196809.
56. Tunnacliffe, E., A.M. Corrigan, and J.R. Chubb, Promoter-mediated diversification of transcriptional bursting dynamics following gene duplication. Proceedings of the National Academy of Sciences, 2018. **115**(33): p. 8364-8369.
57. Miermont, A., et al., The fate of cells undergoing spontaneous DNA damage during development. Development, 2019. **146**(12): p. dev174268.
58. Crocker, J.C. and D.G. Grier, Methods of digital video microscopy for colloidal studies. Journal of colloid and interface science, 1996. **179**(1): p. 298-310.
59. Meyer, F., Topographic distance and watershed lines. Signal processing, 1994. **38**(1): p. 113-125.
60. Ester, M., et al. A density-based algorithm for discovering clusters in large spatial databases with noise. in kdd. 1996.